



CFD simulations of the effects of small dispersed bubbles on the rising of a single large bubble in 2D vertical channels

Jinsong Hua*

Department of Computational Materials Processing, Institute for Energy Technology, PO Box 40, NO-2027, Kjeller, Norway



HIGHLIGHTS

- A framework for modeling two-phase flows with multiple length-scale structures was proposed.
- The couplings among the phases of different length-scales are accounted for.
- Both hindrance and acceleration effects on large bubble rising are revealed.
- The simulation results agree with experimental observations qualitatively.

ARTICLE INFO

Article history:

Received 11 July 2014

Received in revised form

14 October 2014

Accepted 15 October 2014

Available online 27 October 2014

Keywords:

Multiphase flow

Bubble interaction

Computational fluid dynamics

VOF method

DPM method

ABSTRACT

A computational fluid dynamics based numerical model framework was proposed to simulate two-phase flows with interfacial structures of multiple length-scales, e.g. one large bubble and many small dispersed bubbles. In this numerical method, the large bubble is tracked using a volume of fluid (VOF) method, and the small bubbles are tracked using a discrete particle method (DPM). The couplings among the continuous liquid/gas phases and the discrete small bubble phases are accounted for. To evaluate the model performance, this model was applied to simulate the interaction between a large bubble and many suspended small bubbles in 2D vertical channels under different bubble shape regimes. It is found that the small dispersed bubbles may impose important effects on the rising behavior of the large bubble. The simulations have revealed both hindrance and acceleration effects of small bubbles on the rising of large bubble, which agrees with experimental observations qualitatively.

© 2014 Elsevier Ltd. All rights reserved.

1. Introduction

The dynamics of bubbles rising in viscous liquids due to buoyancy is relevant to many industrial processes, such as oil/gas transport, bubble columns and boiling flows. Most of these bubbly flow systems consist of multiple bubbles with different sizes. The interactions among these bubbles impose important effects on the flow behavior. Especially, the effects of small dispersed bubbles on the rising behavior of a large bubble can be significant, and these effects are not understood well so far.

The rising of a single gas bubble in a viscous liquid has been investigated extensively through theoretical analysis (Davies and Taylor, 1950), experiments (Clift et al., 1978; Bhaga and Weber, 1981; Tomiyama et al., 2002a) and numerical simulations (Hua and Lou, 2007; Hua et al., 2008). In the experiments, the complex behaviour of the rise of a single bubble has been observed and recorded. With the rapid development of CFD based numerical

modelling techniques for interface tracking technology in two phase flows such as the Front Tracking method, the VOF method and the level set method, the terminal bubble shape and rising speed can be predicted well in most flow regimes. Our physical understanding of a single bubble rising in liquid has been reasonably established.

To understand the effects of bubble interaction, both experiments (Stewart, 1995; Garnier et al., 2002; Simonnet et al., 2007) and numerical simulations (Krishna et al., 1999; Smolianski et al., 2008; Roghair et al., 2011; Yu et al., 2011) have been applied to investigate multiphase flow systems with a limited number of bubbles of similar size. The early experiments by Stewart (1995) focused on the interactions of freely rising ellipsoidal bubbles. A video camera following the rising bubbles was used to record the dynamics of the bubble interactions during approach, contact, coalescence or break up. It was found that a bubble contacts another by following its wake, which leads to an overtaking collision. Several interacting bubbles may form a dynamic cluster, which accelerates the overall bubble rise speed. Garnier et al. (2002) studied the rise of a homogeneous dispersion of gas bubbles in water. A special design was adopted in the experiments

* Corresponding author. Tel.: +47 4654 3182; fax: +47 6381 1168.
E-mail address: jinsong.hua@ife.no

to limit bubble coalescence and maintain mono-distribution of bubble size. They found that the mean bubble rise velocity decreases when the void fraction increases, due to bubble interactions. This is well known as the hindrance effect. Similarly, the experiments by Simonnet et al. (2007) studied the influence of the void fraction on the relative velocity of a swarm of gas bubbles in a bubble column. The bubble diameters varied from 2 to 10 mm, and local void fraction could be as high as 35%. It was found that when the local void fraction is smaller than 15%, the relative bubble velocity is determined by the hindrance effect, and consequently decreases with the local void fraction. On the other hand, when the local void fraction is higher than 15%, the relative bubble velocity begins to be dominated by the acceleration of bubbles in the wake of the leading ones, increasing suddenly with the local void fraction. It should be noted that the bubble size increases with the void fraction in the experiments.

Krishna et al. (1999) studied the rise velocity of a pair of spherical cap bubbles in a bubble column both experimentally and numerically. For the in-line bubble pairs, the trailing bubble rise velocity is enhanced by the wake of the leading bubble. The acceleration factor depends upon the liquid viscosity and separation distance. Roghair et al. (2011) employed a DNS front-tracking model to develop a drag closure for bubble rising in a mono-dispersed bubble swarm with Eötvös numbers in the range of $1 < Eo < 5$, and Morton numbers in the range of $4 \times 10^{-12} < M_o < 2 \times 10^{-9}$. The simulation results showed only hindered rise. Smolianski et al. (2008) performed a numerical study of the rising dynamics of single bubble and bubble swarms in 2D vertical channels with viscous liquids using a level set method. Yu et al. (2011) presented a three dimensional numerical study of the interactions of buoyant bubbles of the same size using a novel lattice Boltzmann method (LBM). Both of their simulations showed that the ellipsoidal bubbles coalesce within a swarm due to bubble-wake interaction, forming large bubbles with a higher rise speed, while spherical bubbles tend to form clusters without coalescence.

Our understanding of the bubble interaction in bubbly flow with uniform bubble size has been established to a certain extent so far. However, in most common industrial bubbly flows, bubbles are not of the same size. The co-existence of different sized bubbles imposes significant challenges in experiments to measure the detailed behavior and flow characteristics for both small bubbles and large bubbles in a multiphase flow system, and we cannot find relevant publications so far. The flexibility in numerical methods provides opportunities to develop new modeling algorithms to simulate the interactions among the small dispersed bubbles and large bubbles in such complex two-phase flows.

There are several possible numerical methods for simulating multiphase flow with interface structures of different length-scales, e.g. a large bubble and many small bubbles. Direct numerical simulation with resolution of all scales of bubbles is one of the possible approaches. Hua et al. (2008) illustrated a simulation of the interactions of two rising bubbles with different sizes using the front tracking method in association with the numerical modeling techniques such as AMR (adaptive mesh refinement) and parallel computing. However, this type of method is not practical for solving the problem with hundreds and thousands of small bubbles. Yan and Che (2010, 2011) and Hänsch et al. (2012) proposed two Eulerian based approaches for such multiphase flows with multiple scales of interfacial structures. Both methods combine the modeling concepts from the interfacial tracking/capturing method (e.g. VOF method) and the multiple-fluid/field model. Although their preliminary trials were very successful, there are still many challenges in resolving the detailed interactions among the different phases. In addition, when the Eulerian approach is applied to the phase of discrete small

bubbles, it is still difficult to include the detailed physics for the discrete bubbles. Alternatively, the hybrid models proposed by Li et al. (1999), van Sint Annaland et al. (2005) and Tomar et al. (2010) track the small dispersed bubbles using a Lagrangian approach. The large-length-scale gas–liquid interface for the large bubble is tracked by a volume of fluid (VOF) in Li et al. (1999) and Tomar et al. (2010), and by a front tracking method in van Sint Annaland et al. (2005). It is believed that the discrete phase model (DPM) is a more natural choice for the small dispersed bubbles. The development of numerical models for the multiphase flow with interfacial structures of multiple length-scales is still in its infancy. Some new modeling concepts and ideas are still under development.

In this paper, a CFD based numerical approach (Li et al., 1999; Tomar et al., 2010), is adopted to investigate the effects of small bubbles on the rising of a single large bubble in a 2D vertical channel. The numerical model is implemented on the platform of a commercial CFD software package, ANSYS Fluent. Both the liquid phase and the gas phase for the large bubble are regarded as one continuous fluid, and the large-length-scale liquid–gas interface between them is tracked using a volume of fluid (VOF) method. The dispersed small bubbles are treated as discrete phase, and tracked using a discrete particle method (DPM). The Navier–Stokes equations for two-phase flow are solved for the viscous liquid and the large gas bubble as one continuous fluid. The trajectories and velocities of the small bubbles are solved in a Lagrangian manner. The two-way momentum coupling between the discrete bubbles and the continuous fluid phase is also taken into account in the simulation. The interaction between the liquid phase and the large bubble through the large-length-scale interface is considered by the VOF model. The direct interaction between the dispersed small bubbles and the large bubble is considered when the small bubbles approach the large-length-scale interface. To focus on the interaction between the large bubble and the small bubbles, a moving reference frame attached to the nose of the large bubble has been implemented.

In the rest of this paper, we first present the comprehensive mathematical description of the model. Then we describe the implementation of the model in the ANSYS Fluent platform with some simplifications due to the technique difficulties and lack of sub-models for some specific mechanisms. We also test model performance based on a 2D laminar multiphase flow system with a large bubble and many small bubbles under different bubble shape regimes. Even though it is still challenging to quantitatively evaluate the model prediction due to the lack of available experimental data, the simulation results are analyzed and compared with the observations in the bubbly flows with uniform bubble size.

2. Mathematical description and CFD implementation

2.1. Model overview and modeling concept

Fig. 1 shows the modeling concept in the proposed model for the multiphase flow with multi-length-scale interface structures. Basically, the multiphase flow system consists of one discrete domain for the dispersed small bubbles, and one continuous fluid domain having a viscous liquid phase and a gas phase for the large bubble. The continuous fluid domain is discretized using a CFD grid. The continuous liquid and gas phases are separated by large-length-scale interfaces. If we assume that it is a sharp interface, a volume color function (ϕ), which is zero for liquid phase and one for gas phase, can be used to differentiate the two phases. Since the small dispersed bubbles are smaller than the CFD grid size, they cannot be resolved by the CFD grid. Hence, they are tracked

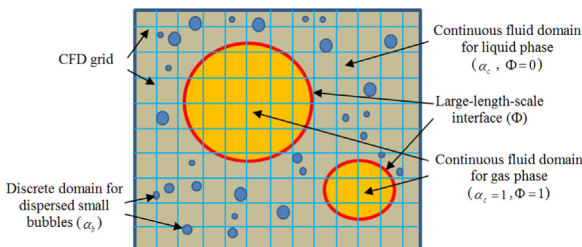


Fig. 1. Schematic diagram of the modeling concept for multiphase flow with multi-length-scale interface structures.

using a Lagrangian method. The small dispersed bubbles co-exist with the liquid phase only ($\Phi = 0$). Hence, if the volume fraction of the small dispersed bubble is α_b , the corresponding volume fraction of the continuous liquid phase should be $\alpha_c = 1 - \alpha_b$. The volume fraction of gas phase ($\Phi = 1$) in the continuous domain is constant as $\alpha_c = 1$ and $\alpha_b = 0$. When the small dispersed bubble approaches the large-length-scale liquid–gas interface, it can either be reflected or penetrate. In the case of penetration, the small bubble will merge with the continuous gas phase. The merge will lead to the interface position adjustment so that the corresponding gas volume fraction of the large bubbles in the continuous fluid domain can keep one ($\alpha_c = 1, \alpha_b = 0, \Phi = 1$). In the case of reflection, the dispersed bubbles will remain in the continuous liquid phase. The trajectories of the small dispersed bubbles depend upon their interaction with the continuous liquid phase. A two-way momentum coupling between the continuous fluid domain and the discrete bubble domain has been implemented in a Lagrangian manner. The large-length-scale interfaces between the large bubbles and the liquid are tracked using a VOF method, and the momentum coupling across the interfaces is considered.

2.2. Governing equations for the continuous fluid domain

The gas/liquid interface in the continuous fluid domain is tracked using a volume of fluid (VOF) method, and a volume colour function (Φ) is used to identify the liquid and gas phases. The two phases can actually be treated as a single fluid whose properties vary in space according to the volume fraction of each phase. Therefore, the fluid density (ρ) and viscosity (μ) in the continuous fluid domain can be estimated as

$$\rho = \rho_G \times \Phi + \rho_L \times \alpha_c \times (1 - \Phi) \quad (1)$$

$$\mu = \mu_G \times \Phi + \mu_L \times \alpha_c \times (1 - \Phi) \quad (2)$$

where α_c is the volume fraction of the continuous fluid phase, and Φ is the volume colour function. The subscripts G and L stand for gas and liquid phases, respectively. It is reasonable to assume that both gas and liquid phases are incompressible under the specified flow conditions in this study. Hence, taking into account the presence of the small dispersed bubbles, the governing equations for the two fluid phases in the continuous domain in a lab reference frame can be formulated.

2.2.1. Continuity equation for gas and liquid phases:

$$\frac{\partial \rho \alpha_c}{\partial t} + \nabla \cdot (\mathbf{u} \rho \alpha_c) = \dot{m}_{DC} \quad (3)$$

where \dot{m}_{DC} is the volumetric source term of the merging rate of small bubbles with the large bubble when the small bubbles penetrate through the large bubble interface.

2.2.2. Momentum equation for gas and liquid phases

$$\frac{\partial \rho \mathbf{u}}{\partial t} + \nabla \cdot (\rho \mathbf{u} \mathbf{u}) = -\nabla p + \nabla \cdot [\mu_e (\nabla \mathbf{u} + \nabla \mathbf{u}^T)] + \mathbf{F}_{ST} + (\rho - \rho_L) \mathbf{g} + \mathbf{F}_{DC} \quad (4)$$

where μ_e is the effective viscosity, including laminar viscosity and turbulent viscosity $\mu_e = \mu + \mu_t$. \mathbf{F}_{ST} stands for the volumetric force for surface tension, \mathbf{F}_{DC} represents the volumetric force from the discrete small bubble phase to the continuous fluid phase due to momentum interaction.

2.2.3. Equation for volume colour function

The volume colour fraction equation (Φ) can be obtained according to the conservation of the continuous gas phase

$$\frac{\partial \Phi}{\partial t} + \nabla \cdot (\mathbf{u} \Phi) = 0 \quad (5)$$

To capture the interface between the gas and liquid phases, the volume colour equation is solved using the geometric reconstruction scheme implemented in ANSYS Fluent. The interface between two fluids is represented using a piecewise-linear approach. The phase volume fraction changes from zero to one across the interface over several grids. The geometric reconstruction scheme can maintain the interface sharpness and minimize numerical smearing of the interface during simulation.

2.3. Governing equations for the discrete phase domain

There are many possible mechanisms for the formation of small bubbles in a multiphase flow system, e.g. gas entrainment, large bubble breakup and small bubble pinch-off. The complex processes are not yet understood well, and there is no physically sound model so far for the prediction of small bubble formation rate, size and distribution. Hence, from the model development point of view, we use certain assumed bubble size, generation rate and distribution for testing the proposed numerical model. As the discrete bubble size is small, we can always assume the bubble shape spherical.

The motion of the small dispersed bubbles is described using a Lagrangian model. The bubble motion in a nonuniform flow field includes translation and rotation. As the bubble size is smaller than the CFD grid size, the effect of bubble rotation is neglected in the bubble dynamic equation. The translation of a small bubble in liquid is governed by Newton's second law as

$$\frac{d}{dt}(m_b \mathbf{u}_b) = \mathbf{F}_b = \mathbf{F}_B + \mathbf{F}_D + \mathbf{F}_L + \mathbf{F}_{VM} \quad (6)$$

where m_b is the mass of the bubble, \mathbf{u}_b represents the bubble velocity, \mathbf{F}_b is the total force acting on the bubble, which may include buoyancy force (\mathbf{F}_B), drag force (\mathbf{F}_D), lift force (\mathbf{F}_L) and added mass force (\mathbf{F}_{VM}).

2.3.1. Buoyancy force (\mathbf{F}_B)

The buoyancy force acting on a bubble is due to the density difference between the bubble and the liquid phase under the gravitational field. It is also referred to as the combined force due to gravity and the far-field pressure. Normally, the buoyancy force can be expressed as

$$\mathbf{F}_B = \frac{m_b}{\rho_b} (\rho_b - \rho_L) \mathbf{g} \quad (7)$$

2.3.2. Drag force (\mathbf{F}_D)

The drag force is one of the most important interaction forces between the dispersed gas bubbles and the bulk liquid. The drag

force is also interpreted as the inter-phase force, and it can be expressed in the following form,

$$\mathbf{F}_D = -K(\mathbf{u}_b - \mathbf{u}) \quad (8)$$

where K is the inter-phase momentum exchange coefficient and can be estimated as

$$K = \frac{1}{2} C_D \alpha_b \alpha_c \rho_L A |\mathbf{u}_{\text{Slip}}| \quad (9)$$

where A is the exposed front area of the bubble moving relative to the liquid, \mathbf{u}_{Slip} is the slip velocity (or relative velocity) between the two phases ($\mathbf{u}_b - \mathbf{u}$), and C_D is the drag coefficient. Various empirical correlations have been proposed to calculate the drag coefficient in the literature. In this study, the following correlation (Ding and Gidaspow, 1990) is selected as it covers a wide range of Reynolds numbers and accounts for the effect of the dispersed small bubble phase,

$$C_D = \begin{cases} \frac{24}{Re_b} [1 + 0.15 \times ((1 - \alpha_b) \times Re_b)^{0.687}] & (1 - \alpha_b)^{-2.65} \\ 0.44 \times (1 - \alpha_b)^{-2.65} & \text{for } \alpha_b \leq 0.2 \text{ and } Re_b < 1000 \\ 2.33 + 200 \frac{\alpha_b}{1 - \alpha_b Re_b} & \text{for } \alpha_b \leq 0.2 \text{ and } Re_b > 1000 \\ & \text{for } \alpha_b > 0.2 \end{cases} \quad (10)$$

where the Reynolds number for the small bubble (Re_b) is defined as

$$Re_b = \frac{D_b |\mathbf{u}_{\text{Slip}}| \rho_L}{\mu_m} \text{ and } \mu_m = \alpha_b \mu_G + (1 - \alpha_b) \mu_L \quad (11)$$

where D_b stands for the bubble diameter, μ_G is the gas viscosity for the dispersed small bubbles. The bubble diameter can be estimated using the bubble mass as $D_b = (6m_b/\rho_b \pi)^{1/3}$. Although the above correlation was developed for rigid spherical particles, it also works well for bubbly flows (Oey et al. 2003).

2.3.3. Lift force (\mathbf{F}_L)

The lift force is another important phase interaction force for bubbly flow. When a dispersed bubble moves in a non-uniform liquid flow field, it experiences a lift force due to vorticity and shear in the liquid flow field. The lift force acting on a dispersed bubble can be expressed as

$$\mathbf{F}_L = -C_L \rho_l V_b (\mathbf{u}_b - \mathbf{u}) \times (\nabla \times \mathbf{u}) \quad (12)$$

where C_L is the lift force coefficient. V_b is the bubble volume. Tomiyama's model (Tomiyama et al., 2002b) is widely used in the literature to calculate the lift coefficient for vertical bubbly flows,

$$C_L = \begin{cases} \min [0.28 \tanh(0.121 Re_b), f(Eo_b)] & Eo_b < 4 \\ f(Eo_b) & 4 < Eo_b < 10 \\ -0.29 & Eo_b > 10 \end{cases} \quad (13)$$

with $f(Eo_b) = 0.00105 Eo_b^3 - 0.0159 Eo_b^2 - 0.0204 Eo_b + 0.474$.

The lift coefficient depends upon the bubble Reynolds number (Re_b), and a modified Eötvös number (Eo_b) that takes into account the bubble deformation. The definition of the modified Eötvös number is given by

$$Eo_b = \frac{g(\rho_L - \rho_G) D_h^2}{\sigma} \quad (14)$$

here D_h is the maximum horizontal dimension of the bubble, and σ is the liquid-gas interface tension coefficient. D_h is calculated using an empirical correlation taking into account bubble deformation,

$$D_h = D_b \sqrt[3]{1 + 0.163 Eo^{0.757}} \quad (15)$$

The Eötvös number is given by

$$Eo = \frac{g(\rho_L - \rho_G) D_b^2}{\sigma} \quad (16)$$

In most cases, the lift force is insignificant compared to the drag force. The lift force is more significant for larger bubbles. Thus, the inclusion of lift forces is not crucial for bubbly flows with very small bubbles.

2.3.4. Virtual mass force (\mathbf{F}_{VM})

The virtual mass force is also known as the added mass force. When a dispersed bubble is accelerated relative to the liquid phase, a "virtual mass" of liquid encountered by the accelerating small bubble exerts a resistance force on the dispersed bubble. For a spherical bubble, the volume of the virtual mass is equal to one-half of the dispersed bubble volume,

$$\mathbf{F}_{VM} = -0.5 V_b \times \rho_L \left(\frac{d\mathbf{u}_b}{dt} - \frac{d\mathbf{u}}{dt} \right) \quad (17)$$

2.3.5. Bubble–bubble collision

In the multiphase flow system, there are may be thousands of small bubbles, and hence Eq. (6) is applied to all small bubbles for calculating their trajectories. The individual small bubble cannot "see" other neighboring bubbles. As a result, the bubbles may overlap each other in the computational domain, which is not physically correct. To avoid the overlapping of small bubbles, the distance between bubbles should be monitored, and a bubble–bubble collision model should be implemented. Due to the complex physics in bubble–bubble interaction, most of the bubble collision models simplified the complexity by treating gas bubbles as hard spheres (Darmana et al., 2006). In fact, the effect of bubble–bubble collisions can be neglected when the concentration of small bubbles is relatively low. At the current stage, the bubble–bubble interaction model was not implemented in this study.

2.4. Interphase couplings

2.4.1. Interphase coupling between liquid and gas phases in the continuous fluid domain

Within the continuous fluid domain, there are two fluid phases: liquid phase and gas phase. They interact with each other through the large-length-scale interface. The Navier–Stokes equations (3) and (4) have included the fluid flow continuity and momentum exchange through the liquid–gas interface. The surface tension can be calculated in terms of volume force as

$$\mathbf{F}_{ST} = \sigma \kappa \nabla \Phi. \quad (18)$$

here σ is the surface tension coefficient, κ is the interface curvature and given by the divergence of the interface unit normal (\mathbf{n})

$$\kappa = \nabla \cdot \mathbf{n} \text{ and } \mathbf{n} = \frac{\nabla \Phi}{|\nabla \Phi|}. \quad (19)$$

2.4.2. Interphase coupling between the discrete phase and liquid phase

The coupling effect of the liquid phase on the motion of individual discrete bubbles has been included in the governing Eq. (6). The effect of the discrete phase on the liquid phase is considered in the governing equations for the continuous domain (4). Here, the distribution of the volume fraction of discrete phase (α_b , $\alpha_c = 1 - \alpha_b$), and the volumetric interaction force by the discrete phase on the continuous domain (\mathbf{F}_{DC}) are needed.

The volume fraction of the discrete bubbles in a CFD grid cell (α_b) is calculated as,

$$\alpha_b = \frac{\sum_i m_{b,i}/\rho_b}{V_{cell}} \quad (20)$$

where i is the number of the small bubbles located in a CFD cell with a volume of V_{cell} . Following Newton's third law, the momentum exchange from the discrete bubbles to the liquid phase is just the opposite of the momentum transfer rate due to buoyancy, drag, lift, and virtual mass forces exerted by the liquid on the bubbles present in a computational cell. Hence, in the computation cell, the volumetric interaction force exerted by the discrete bubbles on the liquid phase can be calculated as

$$\mathbf{F}_{DC} = \frac{\sum_i (-\mathbf{F}_{b,i})}{V_{cell}} \quad (21)$$

2.4.3. Interphase coupling between the discrete bubble and the large-length-scale liquid–gas interface

When a dispersed bubble approaches the large-length-scale liquid–gas interface, it can either penetrate the interface to coalesce with the large bubble or be reflected remaining in the liquid if the interface is assumed sharp. Experimental observations of the interactions between a small bubble and a rigid wall or a free interface were reported in Tsao and Koch (1997) and Sunol and González-Cinca (2010). As suggested by the experimental observation, a small bubble will coalesce with the large bubble when the Weber number is higher than a critical value (We_c), while it will be reflected from the interface when the weber number is lower than the critical value (We_c). The Weber number is defined according to the relative motion of the small discrete bubble to the interface (\mathbf{u}_r) as $We = \rho_l |\mathbf{u}_r|^2 D_b / \sigma$.

As shown in Fig. 2, \mathbf{n} is the local unit normal on the interface. Before the interaction, the normal component of the relative velocity (\mathbf{u}_r) is $\mathbf{u}_{r,n} = -(\mathbf{u}_r \cdot \mathbf{n}) \cdot \mathbf{n}$, and the tangential component of the relative velocity is calculated as $\mathbf{u}_{r,t} = \mathbf{u}_r + (\mathbf{u}_r \cdot \mathbf{n}) \cdot \mathbf{n}$. During the process of interaction, the tangential velocity component is maintained $\mathbf{u}'_{r,t} = \mathbf{u}_{r,t}$, while the normal velocity component is calculated as $\mathbf{u}'_{r,n} = -C_e \mathbf{u}_{r,n}$, where C_e is the restitution coefficient. The restitution coefficient can be a very complicated function of collision velocity, surface tension, bubble size, material properties, surface chemistry, etc. In this study, the collision restitution coefficient is simplified as a constant of 0.8. In numerical implementation, the relative velocity of the small bubble to the interface (\mathbf{u}_r) is difficult to calculate accurately in the VOF method, but it can be approximated using the local slip velocity (\mathbf{u}_{slip}) as the liquid

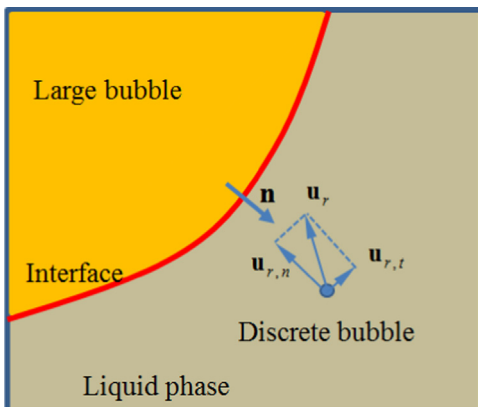


Fig. 2. Schematic diagram of the interaction between a discrete bubble and the large-length-scale interface.

velocity is quite close to the interface velocity in the vicinity of interface.

2.5. Non-dimensionalization for the system of bubble rising in a viscous liquid

To characterize the flow physics better, the following dimensionless variables are introduced to the modeling system,

$$x_i^* = \frac{x_i}{D_B}; \quad u^* = \frac{u}{\sqrt{gD_B}}; \quad t^* = \frac{t}{D_B^{1/2} g^{-1/2}}; \quad \rho^* = \frac{\rho}{\rho_L};$$

$$p^* = \frac{p}{\rho_L g D_B}; \quad \mu^* = \frac{\mu}{\mu_L}; \quad \kappa^* = \frac{\kappa}{D_B^{-1}}$$

where D_B is the equivalent diameter of the large bubble, which can be defined using the bubble volume ((V_B)) as $D_B = (6 \times V_B / \pi)^{1/3}$. Hence, The Navier–Stokes equations for the fluids in the continuous domain can be re-expressed in dimensionless format as

$$\frac{\partial \alpha_c}{\partial t^*} + \nabla \cdot (\mathbf{u}^* \alpha_c) = 0. \quad (22)$$

$$\frac{\partial \rho^* \mathbf{u}^*}{\partial t^*} + \nabla \cdot (\rho^* \mathbf{u}^* \mathbf{u}^*) = -\nabla p^* + \frac{1}{Ar} \nabla \cdot [\mu^* (\nabla \mathbf{u}^* + \nabla \mathbf{u}^{*T})] + \frac{1}{Eo} \kappa^* \nabla \phi + (\rho^* - 1) \frac{\mathbf{g}}{|\mathbf{g}|} + \frac{\mathbf{F}_{DC}}{\rho_L g} \quad (23)$$

Two dimensionless numbers (Archimedes number and Eötvös number) are introduced in the non-dimensionalized governing equation (23),

$$Ar = \frac{\rho_l g^{1/2} D_B^{3/2}}{\mu_L}; \quad Eo = \frac{\rho_l g D_B^2}{\sigma}. \quad (24)$$

Based on the above formulation, the problem of a single bubble rising in viscous liquid can be characterized by four dimensionless parameters, namely the density ratio (ρ_G/ρ_L), the viscosity ratio (μ_G/μ_L), the Archimedes number (Ar) and the Eötvös number (Eo), which can be used as the input parameters for problem setup. In many publications, another dimensionless number called the Morton number is also used to characterize two-phase flow systems,

$$Mo = \frac{g \mu_L^4}{\rho_L \sigma^3} = \frac{Eo^3}{Ar^4}. \quad (25)$$

In most experimental studies of bubble rising in viscous liquid, the Reynolds number based on the terminal bubble rising speed (U_B) is used to present the bubble rising characteristics:

$$Re = \frac{\rho D_B U_B}{\mu_L}. \quad (26)$$

The terminal bubble rising speed can also be non-dimensionalized as a Froude number, $Fr = U_B / (g D_B)^{1/2}$. Hence, the Reynolds number can be correlated with the Archimedes number as $Re = Ar \times Fr$.

2.6. Moving reference frame

In order to focus our attention on the interaction between the large bubble and the discrete small bubbles and use a relatively small computational domain for the moving bubbles, a moving reference frame attached to the large bubble nose is implemented. The description of the numerical implementation of the moving reference frame can be found in Hua et al. (2008, 2012).

2.7. Model implementation in ANSYS Fluent

The model described above has been implemented in ANSYS Fluent based on the combination of two multiphase models: the Volume of Fluid (VOF) method and the Discrete Particle Method (DPM). In addition, User Defined Functions (UDF) are coded to customize the generic commercial CFD code so that the special function requirements and boundary conditions for the new model can be implemented. Although we can achieve most of the functionalities for the new model, we face some technical challenges in some aspects. For example, we have not found an acceptable way to implement the bubble–bubble collision model for the small dispersed bubbles. As a result, the discrete bubbles have the possibility of overlapping in the computational domain. When the small bubble concentration is high, this may lead to unphysical simulation results, and instability of the numerical method. When the discrete bubble phase is dilute, its effect is not so important.

To evaluate the model performance, we design a simulation case to investigate the effect of small bubbles on the rise of a single large bubble in quiescent viscous liquid in a 2D vertical channel as shown in Fig. 3. As the system is normalized by the equivalent radius of the large bubble (D_B), the channel width is about $2.5D_B$, and the channel height is about $10D_B$. The initial bubble nose (the highest point on the bubble surface) is located at $2D_B$ away from top inlet of the channel. As a moving reference frame is attached to the bubble nose, the bubble nose position is fixed in the computational domain during the transient simulation. If the large bubble rise velocity is U_B , the liquid inlet velocity at the channel top is set as $U_L = -U_B$, and the channel wall velocity is set as $U_w = -U_B$. The discrete bubbles are released into the flow system at seven particle injection points located at the upper part of the channel very close to the top inlet. It is assumed that the small bubbles are spherical with a diameter of $0.025D_B$. The bubble injections occur at every simulation time step with a total mass rate of \dot{m}_{PI} . It can be non-dimensionalized as $\dot{M}_{PI} = \dot{m}_{PI}/\rho_G D_B^{5/2} g^{1/2}$. In the simulation the

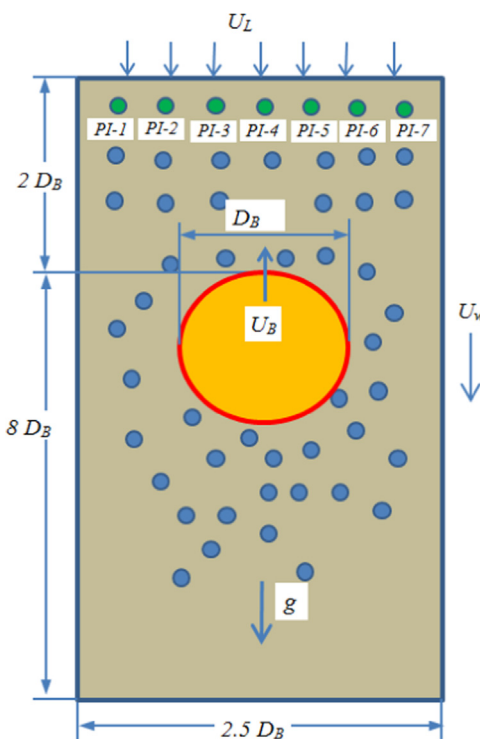


Fig. 3. Schematic diagram for modelling the interaction between the small bubbles and a rising large bubble in a vertical channel with viscous liquid.

density ratio is set as $\rho_G/\rho_L = 0.001$, and viscosity ratio $\mu_B/\mu_L = 0.01$. The Archimedes number (Ar) and Eötvös number (Eo) are varied in the simulations in different bubble shape regimes.

In addition, when the mass flux of the discrete phase is set to zero (\dot{M}_{PI}), or the momentum coupling from the discrete domain to the continuous domain is turned off, the small bubbles will behave as tracer bubbles. In this case, the small bubbles will be driven by the flow field in the continuous domain, but they impose no effects on the flow field in the continuous domain.

3. Results and discussion

3.1. Review of single bubble rising in an infinite fluid

The rising of a single bubble in an infinite viscous fluid has been studied extensively using various possible approaches: theoretical analysis, experiments and numerical simulations. The variations of bubble terminal shape and bubble terminal velocity under different flow conditions have been a common research focus. For example, Grace (1973) analyzed the experimental data on bubble shapes and rising velocities in quiescent viscous liquid and showed that the data can be condensed into one diagram, provided that appropriate dimensionless numbers are used. A copy of this diagram taken from Clift et al. (1978) is reproduced in Fig. 4, which shows the experimental observed bubble shapes for different Reynolds numbers, Eötvös numbers and Morton numbers. The observed typical bubble shape regimes include spherical, oblate ellipsoidal, spherical cap, skirted bubble and wobbling bubbles. A good understanding of bubble shape regimes has been established, and this has been widely accepted as the benchmark experiments to evaluate the performance of newly development multiphase flow models.

As most available experimental data related to bubble interaction are for homogeneous bubbly flow, and there are very few experimental data on the interaction between a cluster of very small bubbles and a large bubble. Hence, the bubble shape regime

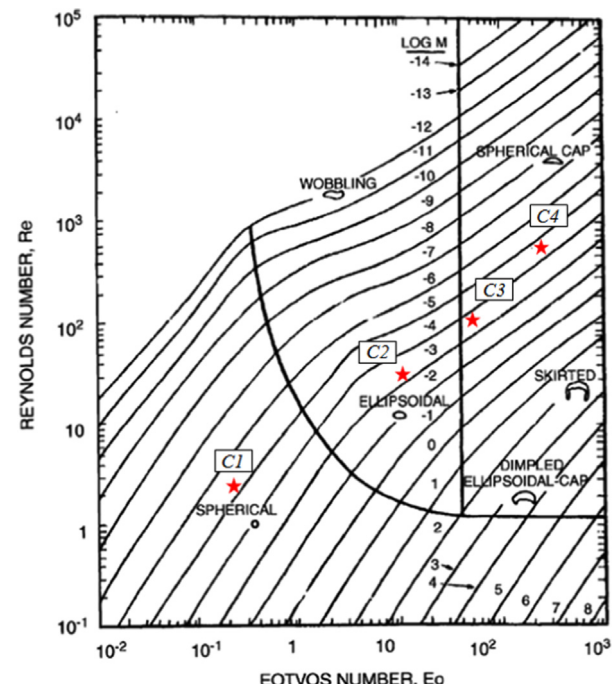


Fig. 4. Bubble diagram of Grace (1973) for the shape and terminal rise velocity of gas bubbles in quiescent viscous liquids.

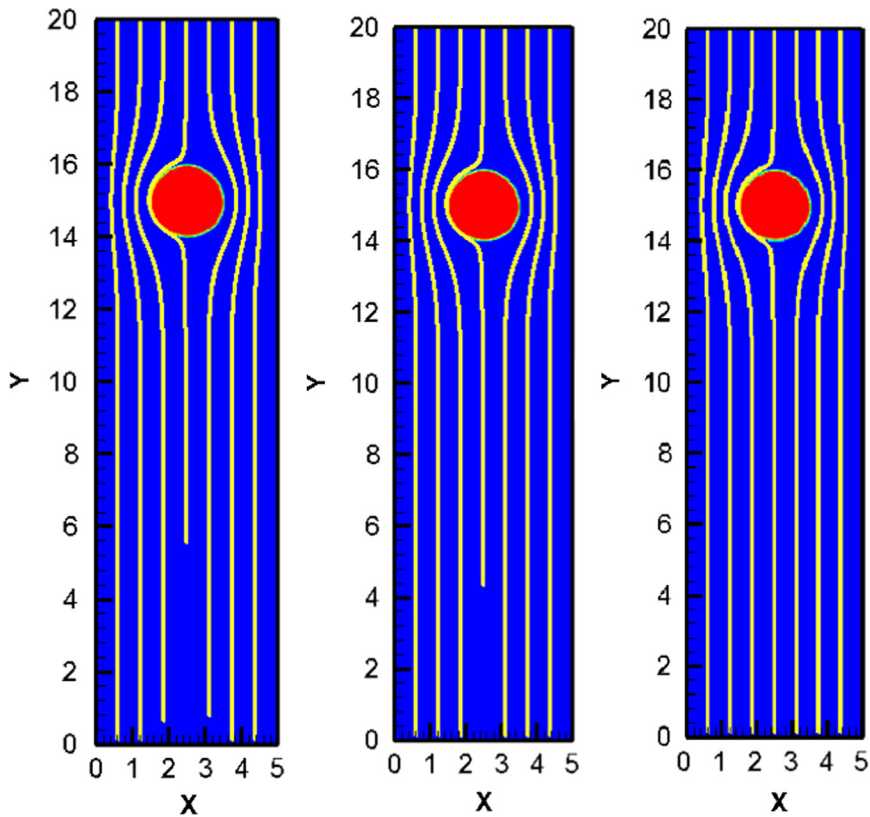


Fig. 5. Snapshots of predicted shape of the large bubble and trajectories of small tracer bubbles for $Ar = 5.66$, $Eo = 0.2$, $\dot{M}_{Pl} = 0$. $Fr_{B,0} = 0.175$.

diagram shown in Fig. 4 is used as a reference to select the flow conditions for the further study. As represented by the stars in Fig. 4, four simulation cases in different bubble shape regimes are selected. The parameters for these four simulation cases are: Test Case 1-spherical ($Ar = 5.66$, $Eo = 0.2$, $Mo = 7.8 \times 10^{-6}$); Test Case 2-oblate ellipsoidal ($Ar = 28.3$, $Eo = 8$, $Mo = 8.4 \times 10^{-4}$); Test Case 3-spherical cap with flat bottom ($Ar = 141.4$, $Eo = 40$, $Mo = 1.6 \times 10^{-4}$); Test Case 4-spherical cap with dimpled bottom ($Ar = 565.7$, $Eo = 200$, $Mo = 7.8 \times 10^{-5}$).

3.2. Test Case 1-spherical bubble

Under the flow conditions of $Ar = 5.66$ and $Eo = 0.2$, the terminal shape of the large bubble is approximately spherical. Fig. 5 shows some snapshots of the large bubble shape and the tracer bubble trajectories ($\dot{M}_{Pl} = 0$). A steady state of bubble shape and position can be obtained in the simulation. The large bubble remains spherical and on the channel central symmetric line. The small tracer bubbles follow the flow streamlines. The tracer bubbles released at the channel center meet the stagnation point at the large bubble's nose, slide to one side of the bubble, fall along the bubble surface and separate from the bubble at the bottom. This indicates that there is no wake present under the large bubble at such low Archimedes number and Eötvös number. The terminal rise velocity of the large bubble can be expressed in terms of Froude number $Fr_{B,0} = 0.175$.

When the total dimensionless mass release rate of small bubbles is set to $\dot{M}_{Pl} = 0.0247$, the momentum exchange between the discrete small bubbles and the continuous fluid takes effect as shown in Fig. 6. Although the large bubble shape shows no significant change, its position starts to oscillate in the lateral direction. This can be clearly seen from the trajectories of the small bubbles released at the channel center. Compared to the trajectories shown in Fig. 5, the small bubbles released at the center-line

meet the large bubble near the stagnation point and slide to either side of the bubble alternatively as the large bubble oscillates laterally. Although the small bubbles can fall down along the bubble surface, the separation at the large bubble bottom becomes difficult. Some of them are trapped under the large bubble and shed off later, forming a relatively concentrated region in the channel center under the large bubble. As a result, the large bubble rise speed is predicted as $Fr_B = 0.161$, which is lower than the case with tracer small bubbles. This indicates that the presence of small bubbles slows down the rising speed of the large bubble. The overall average volume fraction of small bubbles is about $\alpha_b = 12.5\%$.

When the total dimensionless mass release rate of small bubbles is increased to $\dot{M}_{Pl} = 0.0619$, the interaction between the discrete bubbles and the continuous fluid phase becomes stronger as shown in Fig. 7. The shape of the large bubble is deformed further as slightly oblate ellipsoidal, and it oscillates laterally from side to side. Some sort of aggregation process occurs in the discrete bubble phase, forming some bubble clusters. The small bubble cluster follows the large bubble for some period of time and is shed off later on. The large bubble rise speed is slowed down further to $Fr_B = 0.146$, and more small bubbles tend to accumulate around the large bubble. As a result, the overall average volume fraction of the small bubbles becomes higher as $\alpha_b = 24.5\%$. Without a bubble–bubble collision model, the small discrete bubbles with high volume fraction may overlap each other in some zones, which will reduce the simulation accuracy of the DPM model.

3.3. Test Case 2-oblate ellipsoidal bubble

Under the flow conditions of $Ar = 28.3$ and $Eo = 8$, the terminal shape of the large bubble, which rises in the quiescent viscous liquid without small bubbles, is ellipsoidal. Fig. 8 shows the effects

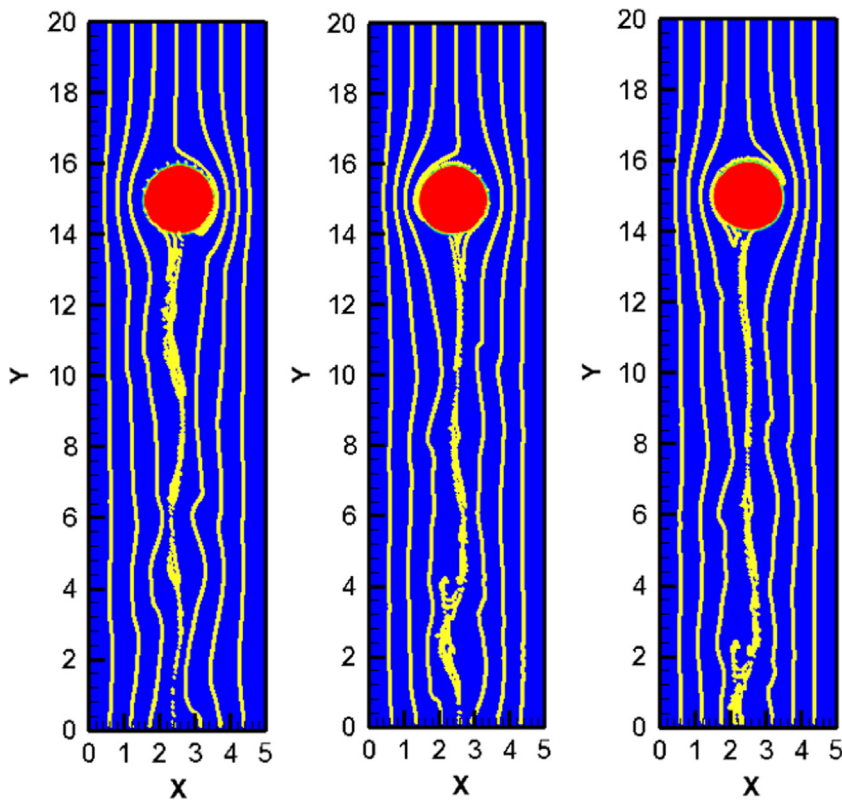


Fig. 6. Snapshots of predicted shape of large bubble and trajectories of small bubbles for $Ar = 5.66$, $Eo = 0.2$, $\dot{M}_{Pl} = 0.0247$, $Fr_B = 0.161$, $\alpha_b = 12.5\%$.

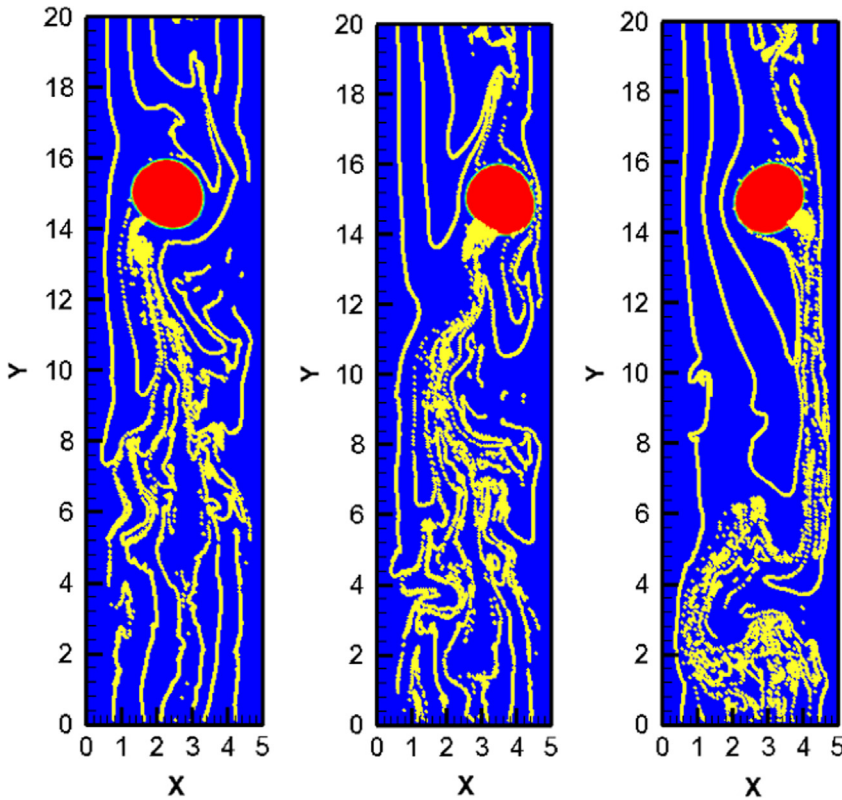


Fig. 7. Snapshots of predicted shape of large bubble and trajectories of small bubbles for $Ar = 5.66$, $Eo = 0.2$, $\dot{M}_{Pl} = 0.0619$, $Fr_B = 0.146$, $\alpha_b = 24.5\%$.

of the large bubble on the trajectories of the small tracer bubbles ($\dot{M}_{Pl} = 0$). Generally, the tracer bubbles follow the flow streamlines around the large bubble. The small bubbles released at the channel center will meet the bubble nose, slip towards either side of the

bubble alternatively, follow the bubble surface going downwards, and separate smoothly from the bubble bottom. It seems that no small bubbles are trapped under the large bubble. The predicted rise velocity of the large bubble is about $Fr_{B,0} = 0.339$.

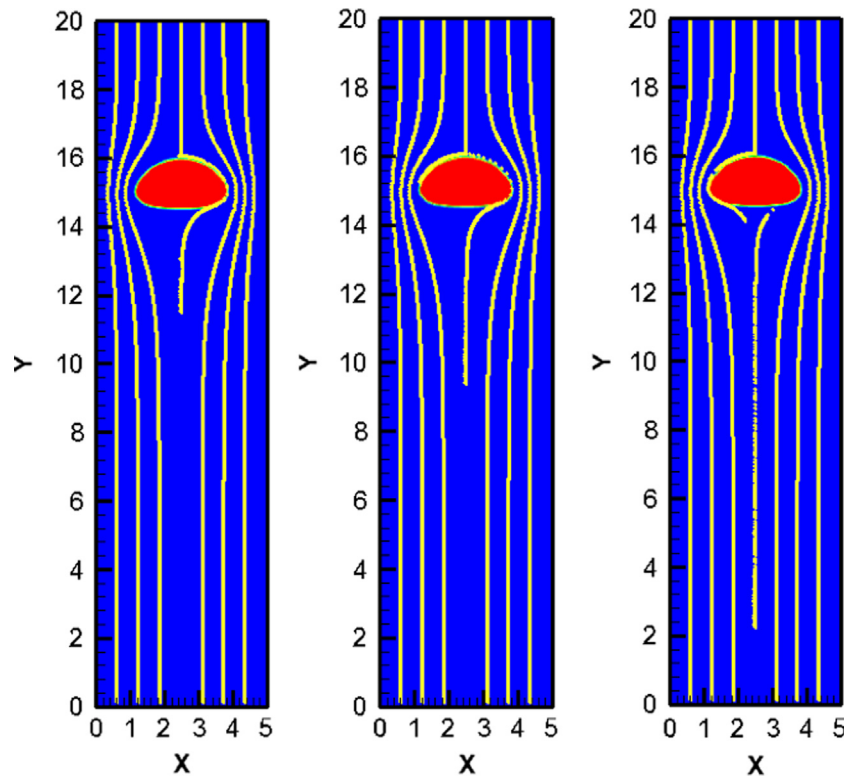


Fig. 8. Snapshots of predicted shape of large bubble and trajectories of small tracer bubbles for $Ar = 28.3$, $Eo = 8$, $\dot{M}_{Pl} = 0$. $Fr_{B,0} = 0.339$.

When the mass release rate of small bubbles is set to $\dot{M}_{Pl} = 0.0247$, the momentum interaction between the discrete bubble phase and the continuous phase imposes significant effects on both phases. As shown in Fig. 9, the large bubble becomes a little sharper at the bubble nose, and tilts and oscillates while rising in the channel. A significant wake zone is created under the large bubble. The trajectories of small bubbles are significantly affected by the large bubble, especially for those released at the channel center. They meet the large bubble at the nose region. As the large bubble tilts and waves from side to side, the meeting point on the large bubble also varies from side to side. The small bubbles slip downwards along the bubble surface, and most of them are trapped in the wake zone of the large bubble. As these small bubbles rise with the large bubble, some of them will be shed off the wake zone. The large bubble rise speed is increased to $Fr_B = 0.35$. This indicates that the presence of small bubble increases the rise speed of the large bubble under this flow condition.

When the mass release rate of small bubbles is increased further to $\dot{M}_{Pl} = 0.0619$, the discrete small bubbles have a stronger effect on the large bubble rise. The nose of the large bubble becomes much sharper as shown in Fig. 10. The large bubble remains tilted and waves from one side to the other while rising. The terminal rise speed of the large bubble increases further to $Fr_B = 0.379$. The small bubbles have a high probability of being trapped by the wake of the large bubble and shed off later. It seems that small bubble aggregation occurs as the concentration goes up. The overall average volume fraction of small bubbles is about $\alpha_b = 14.3\%$.

3.4. Test Case 3-spherical cap bubble with flat bottom

Under the flow conditions of $Ar = 141.4$ and $Eo = 40$, the terminal shape of the large bubble will be a spherical cap with a flat bottom while it rises in a quiescent viscous liquid. Fig. 11

shows the trajectories of small tracer bubbles around the large bubble. A significant open wake zone with two unbalanced flow vortices is formed under the large bubble. When the recirculation zone at one side grows big enough, it will be shed off. Then the recirculation zone at the other side starts to grow quickly. The bubble bottom oscillates as the dominant recirculation zone shifts from one side to other. A vortex street is formed under the large bubble through the vortex shedding process. The small bubbles released at the channel center are more easily trapped in the bubble wake zone. The strong mixing of the vortex street finally gets the small bubbles to follow the liquid flow pattern.

As shown in Figs. 12–14, the mass release rates for small bubbles are increased from $\dot{M}_{Pl} = 0.00124$ to $\dot{M}_{Pl} = 0.0124$, the effect of small bubbles on the large bubble rising becomes more and more significant, while the effect of large bubble on the small bubble distribution has no significant change.

As the mass release rate increases, more small bubbles will be present in the liquid. The shape of the large bubble is deformed significantly as shown in Figs. 13 and 14. The large bubble nose becomes much sharper, and the bubble bottom becomes more unstable. The large bubble behaves, to a certain extent, like a wobbling bubble. All these changes are related to the significant increase of the large bubble rise speed.

As shown in Figs. 12–14, the distribution patterns of the small bubbles are not significantly changed by the increase of the mass release rate for small bubbles. The strong mixing caused by the vortex street always leads to a more even distribution of small bubbles inside the channel, especially when the time average is considered. Even though the amount of small bubbles is increased significantly by changing the mass release rate from $\dot{M}_{Pl} = 0.00124$ to $\dot{M}_{Pl} = 0.0124$, the volume fraction of small bubbles is still relatively low (less than 3%) inside the computational domain. This will result in minor changes to the general liquid flow pattern induced by the large bubble, but the large bubble rise speed is increased significantly.

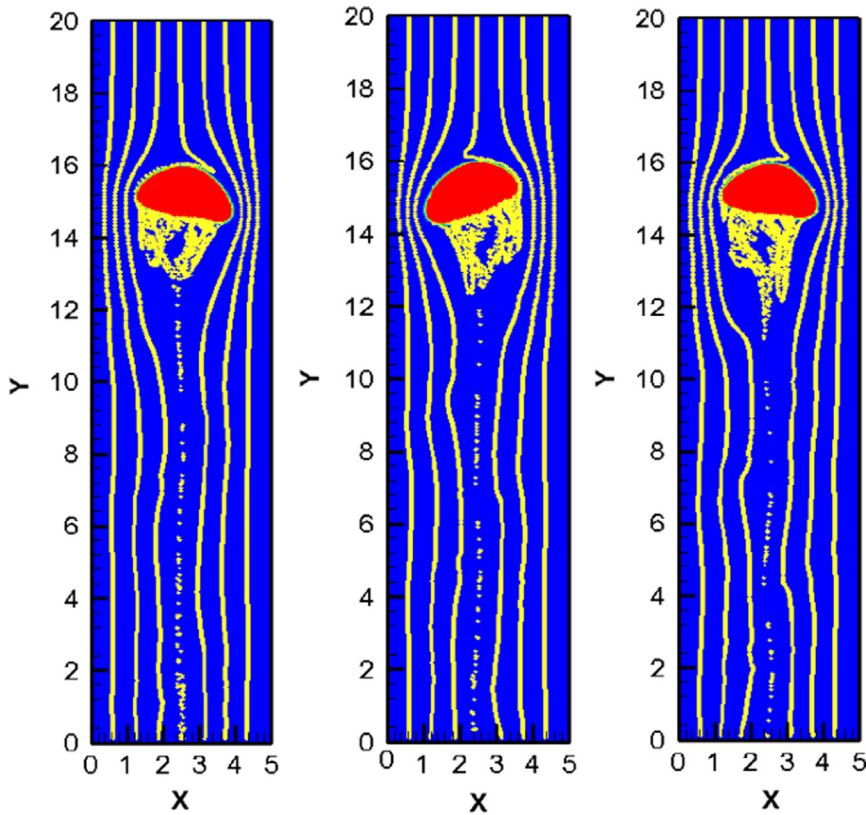


Fig. 9. Snapshots of predicted shape of large bubble and trajectories of small bubbles for $Ar = 28.3$, $Eo = 8$, $\dot{M}_{Pl} = 0.0247$, $Fr_B = 0.35$, $\alpha_b = 5.91\%$.

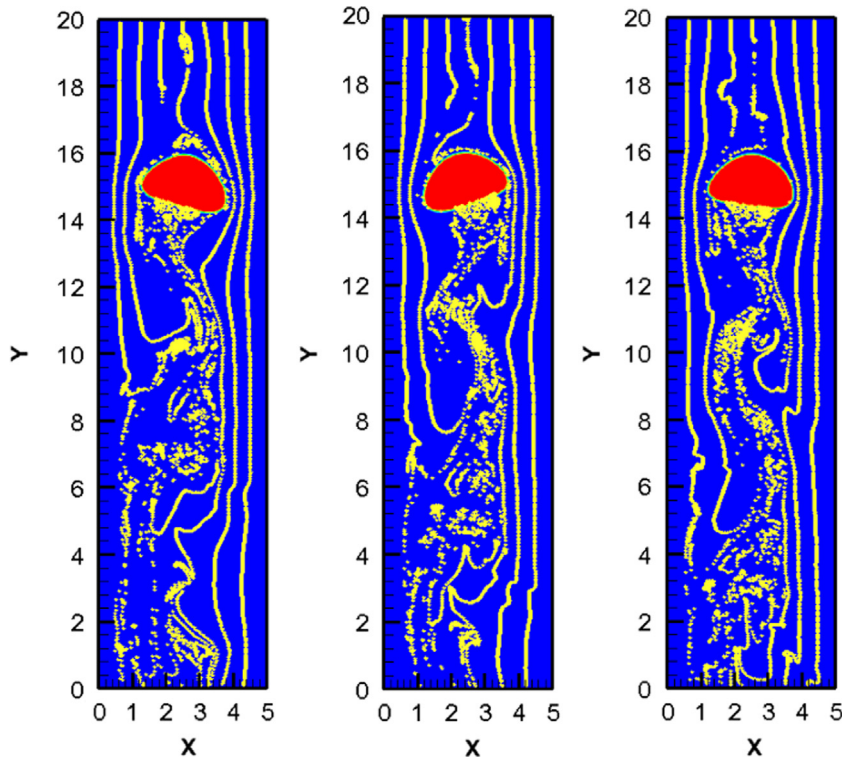


Fig. 10. Snapshots of predicted shape of large bubble and trajectories of small bubbles for $Ar = 28.3$, $Eo = 8$, $\dot{M}_{Pl} = 0.0619$, $Fr_B = 0.379$, $\alpha_b = 14.3\%$.

3.5. Test Case 4-spherical cap bubble with dimpled bottom

Under the flow conditions of $Ar = 565.7$ and $Eo = 200$, the large bubble is in the shape of a spherical cap with a dimpled bottom for a rising bubble in quiescent viscous liquid. As shown in Fig. 15, the

large spherical cap bubble waves significantly while rising. The maximum tilt angle can reach about 45° . A strong vortex is shed off every time when it changes the tilt direction. Sometimes, some small bubbles are pinched off at the sharp corner of the spherical cap. This leads to the shrinkage of the large bubble size in the

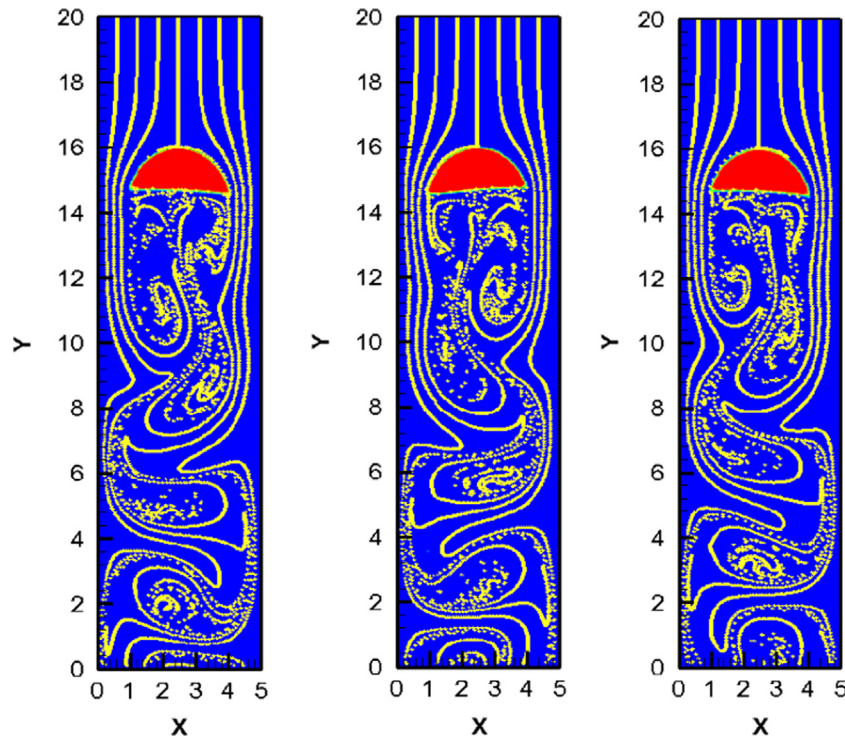


Fig. 11. Snapshots of predicted shape of large bubble and trajectories of small tracer bubbles for $Ar = 141.4$, $Eo = 40$, $\dot{M}_{Pl} = 0$. $Fr_{B,0} = 0.348$.

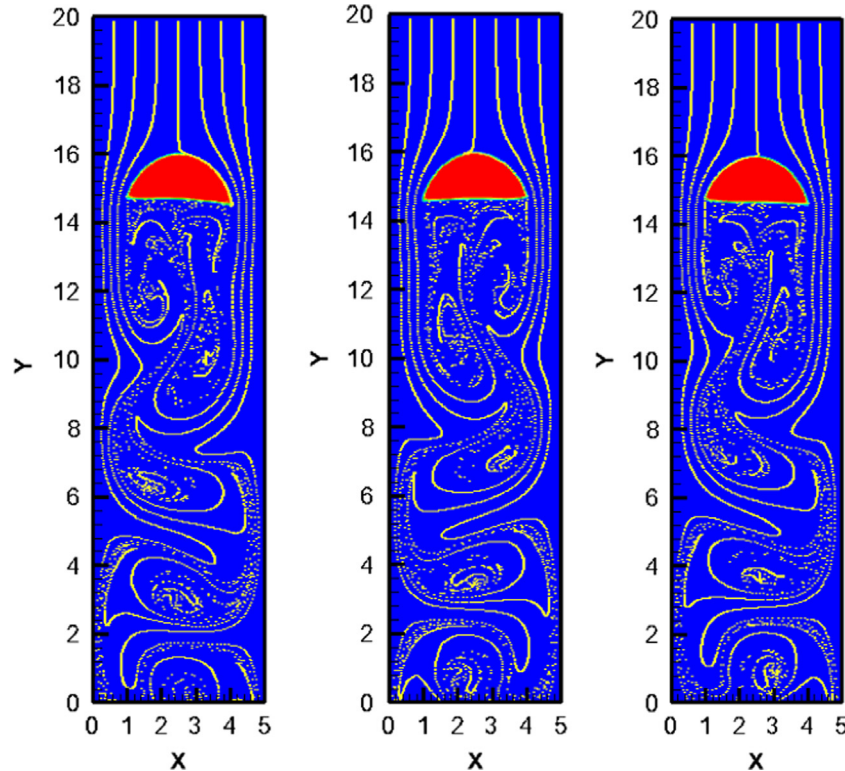


Fig. 12. Snapshots of predicted large bubble shape and trajectories of small bubbles for $Ar = 141.4$, $Eo = 40$, $\dot{M}_{Pl} = 0.00124$. $Fr_B = 0.358$, $\alpha_b = 0.279\%$.

simulation. Some of the pinched off small bubbles, if they are large enough, can be tracked by the VOF method. The strong vortices mix the downstream flow quickly. After about four vortex structures, the small bubbles become almost evenly distributed across the channel.

When the small tracer bubble is replaced by the bubbles which have the two-way momentum exchange with the continuous

liquid, the small bubbles start to impose some effect on the rising behavior of the large bubble. Fig. 16 shows the snapshots of the predicted shape of large bubble and distribution of small bubbles, when the mass release rate of small bubbles is set to $\dot{M}_{Pl} = 0.00124$. The front of the large bubble becomes sharper, especially at the location where the small bubble stream meets the large bubble. The effect becomes more significant when the mass

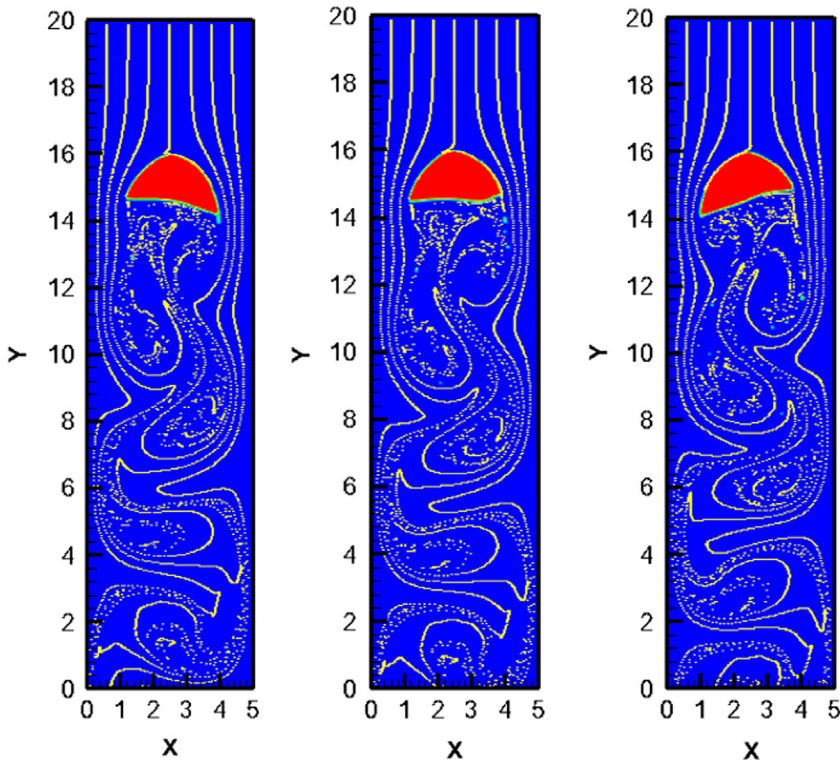


Fig. 13. Snapshots of predicted large bubble shape and trajectories of small bubbles for $Ar = 141.4$, $Eo = 40$, $\dot{M}_{pl} = 0.00619$, $Fr_B = 0.417$, $\alpha_b = 1.24\%$.

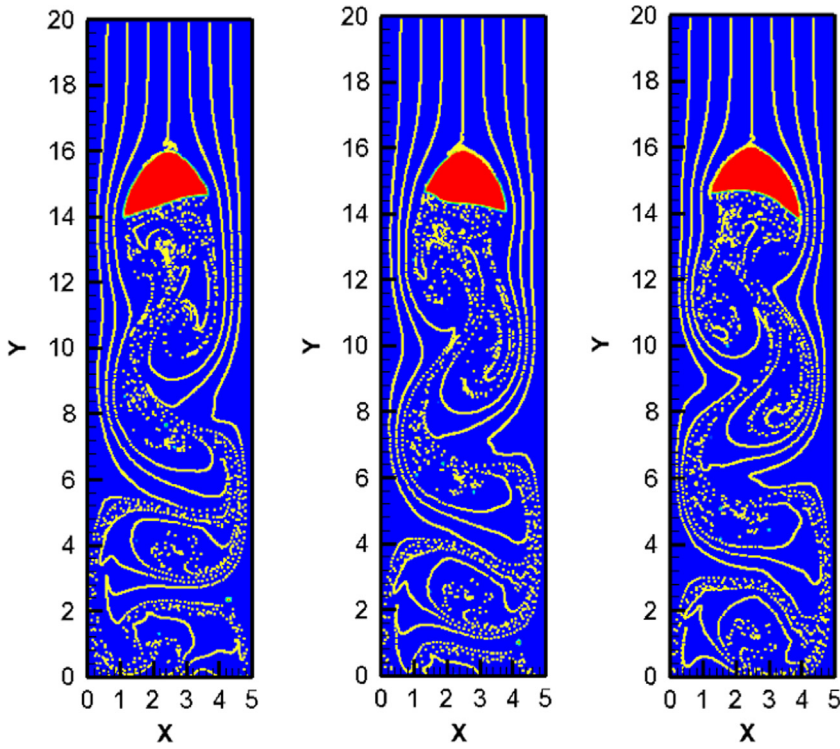


Fig. 14. Snapshots of predicted shape of large bubble and trajectories of small bubbles for $Ar = 141.4$, $Eo = 40$, $\dot{M}_{pl} = 0.0124$, $Fr_B = 0.468$, $\alpha_b = 2.17\%$.

release rate of the small bubbles is increased to $\dot{M}_{pl} = 0.00619$ as shown in Fig. 17. Another consequence of increasing the mass release rate of small bubbles is that the rise speed of the large bubble increases from $Fr_B = 0.379$ to $Fr_B = 0.508$. However, the distribution of small bubbles is not affected heavily by the

increased mass release rate of small bubbles, even though the average volume fraction of small bubbles increases from $\alpha_b = 0.0265\%$ to $\alpha_b = 1.03\%$. The strong mixing caused by the flow vortex after the large bubble leads to a more even distribution of small bubbles.

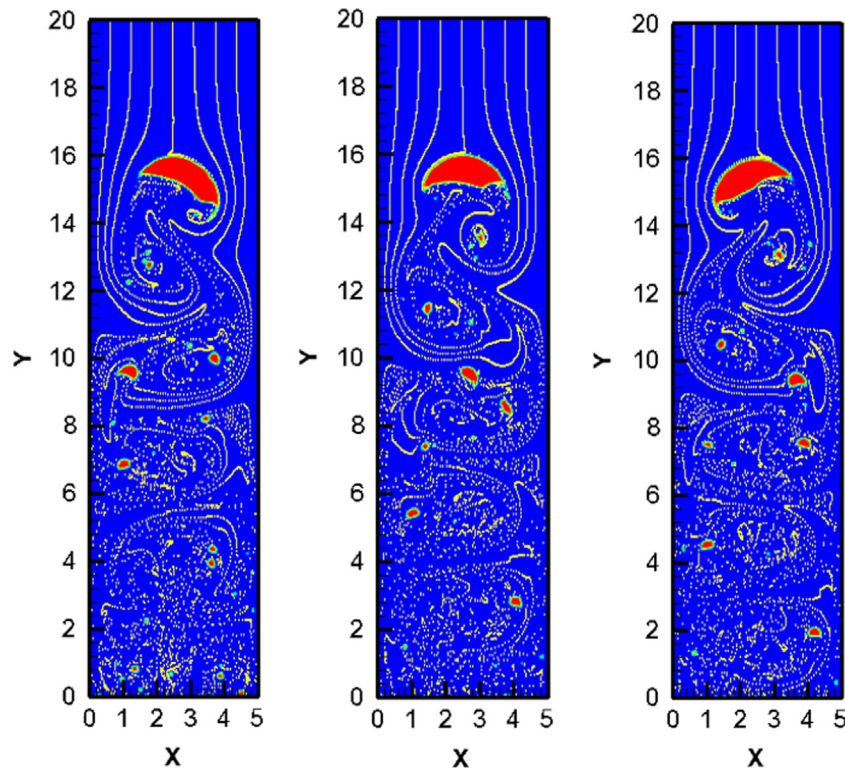


Fig. 15. Snapshots of predicted shape of large bubble and trajectories of small tracer bubbles for $Ar = 565.6$, $Eo = 200$, $\dot{M}_{Pl} = 0$, $Fr_{B,0} = 0.349$.

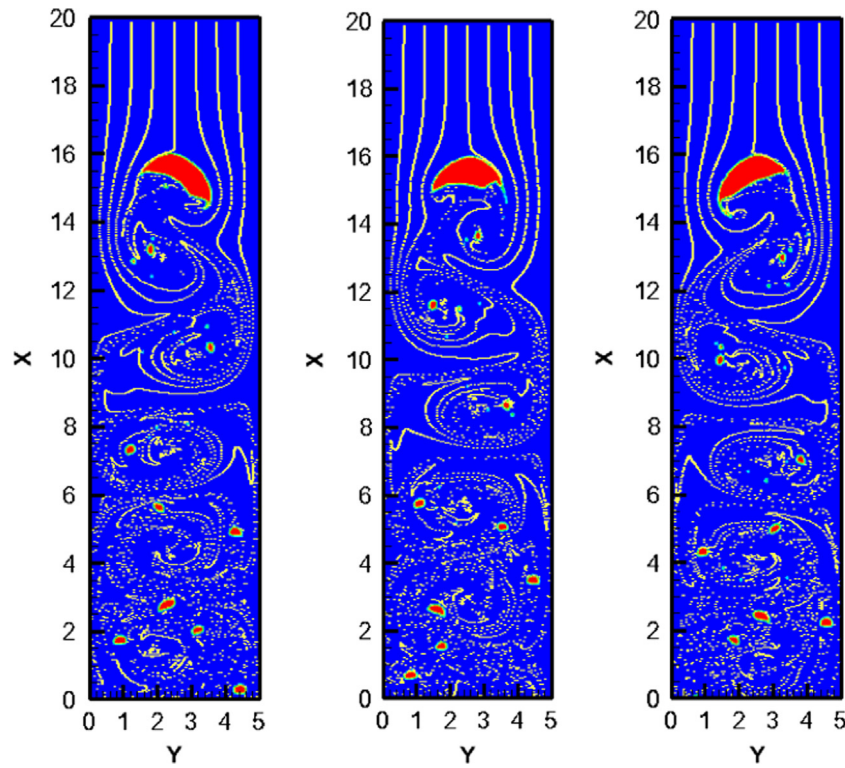


Fig. 16. Snapshots of predicted shape of large bubble and trajectories of small bubbles for $Ar = 565.7$, $Eo = 200$, $\dot{M}_{Pl} = 0.00124$, $Fr_B = 0.379$, $\alpha_b = 0.0265\%$.

3.6. Effect of small bubbles on the large bubble rise speed

The variation of the rise speed of the large bubble with the volume fraction of small bubbles is shown in Fig. 18 for the bubble shape regimes of spherical and oblate ellipsoidal with relatively low Archimedes numbers and Eötvös numbers. It is clearly shown

in Fig. 18 that the rise speed of the large bubble decreases as the volume fraction of small bubbles increases when the large bubble is near spherical with very low Archimedes number and Eötvös number ($Ar = 5.66$, $Eo = 0.2$). Similar phenomena are observed in homogeneous bubbly flow with mono-dispersed bubbles due to the hindrance effect. The hindrance effect has been observed and

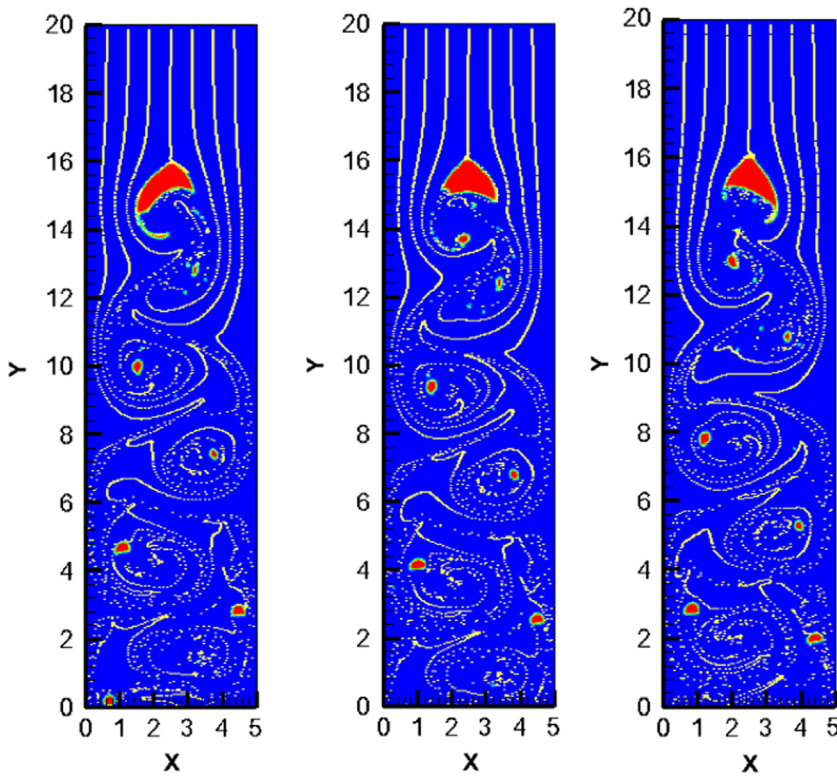


Fig. 17. Snapshots of predicted shape of large bubble and trajectories of small bubbles for $Ar = 565.7$, $Eo = 200$, $M_{pl} = 0.00619$, $Fr_B = 0.508$, $\alpha_b = 1.03\%$.

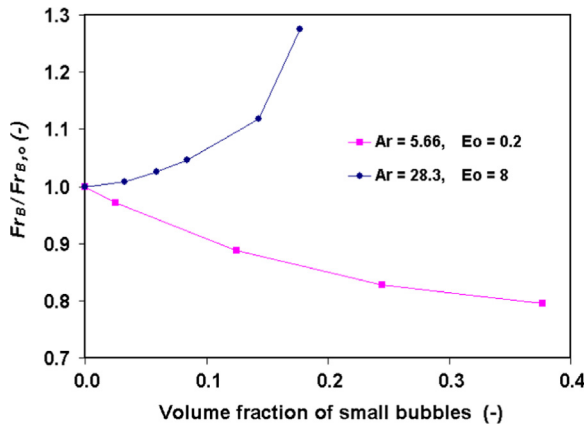


Fig. 18. Variation of the rise speed of large bubble with the volume fraction of small bubbles at relatively low Archimedes and Eötvös numbers.

reported in experiments (Garnier et al., 2002; Simonnet et al., 2007) and simulation (Roghair et al., 2011). However, the detailed mechanism for the hindrance effect is not well understood so far. The experiments and simulations show that the hindrance effect occurs often in the bubbly flow system with high enough bubble–bubble collision frequency, but the collisions are not strong enough to cause bubble coalescence. In addition, there is no significant wake zone formed behind these interacting bubbles. In the current study, the small bubbles are much smaller than the large bubbles. When more small bubbles are added into the system, the large bubble starts to oscillate laterally and the interactions with the small bubbles are enhanced. Such interactions slow down the vertical rise speed of the large bubble.

On the other hand, when the Archimedes number and Eötvös number are slightly increased ($Ar = 28.3$ and $Eo = 8$), the large bubble is in the oblate ellipsoidal shape regime. The rise speed of

the large bubble increases quickly when the volume fraction of small bubbles goes up. This means that the presence of small bubbles accelerates the rise of the large bubble in the oblate ellipsoidal shape regime. The acceleration of large bubbles in bubbly flow has also been observed in many experiments (Krishna et al., 1999; Simonnet et al., 2007) and simulations (Hua et al., 2008; Smolianski et al., 2008; Yu et al., 2011). A study of the flow conditions indicates that the bubble acceleration occurs mostly for the deformable large bubble with a significant wake zone.

For the condition of Test Case 2 in this study, the large bubble is oblate ellipsoidal in shape and has a significant wake zone while it rises in quiescent liquid. When small bubbles are added to the flow, some of them are trapped in the wake zone as shown in Fig. 9, and the large bubble begins to rise slightly faster due to the additional buoyancy of those small bubbles trapped in the wake zone. When more small bubbles are added to the flow upstream, the large bubble front is affected by the small bubbles and the bubble nose becomes sharper. This deformation of the bubble nose will change the drag force significantly, and the rise speed of the large bubble increases quickly as the volume fraction of small bubbles increases further.

When the Archimedes number and Eötvös number are increased further as in Test Cases 3 and 4 in the spherical cap bubble shape regime, the rise speed of the large bubble increases as the volume fraction of small bubbles goes up. The increase of the large bubble rise speed due to the presence of small bubbles is clearly shown in Fig. 19. Even though the volume fraction of small bubbles is very low (smaller than 2%), their effect on the large bubble rise speed is quite significant with an increase of about 70%. The change of the large bubble rise speed is mainly attributed to the change of bubble shape with a sharper bubble nose as well as vortex shedding behind the large bubble.

Hua et al. (2008) studied the interaction of two different sized bubbles by numerical simulation. The small leading bubble can

impose significant effects on the trailing large bubble. The large trailing bubble first changes its front shape and becomes sharper at the bubble nose, and then accelerates to catch up with the leading small bubble. Before the coalescence, the rise speeds of the two bubbles go up. Similar conclusion can also be obtained from the simulation results of Krishna et al. (1999) and have been observed in experiments (Stewart, 1995). In another simulation case of Hua et al. (2008), when a small bubble is sucked into the wake of a large bubble, the small bubble has a minor effect on the rise speed of the large bubble. This agrees with the simulation results of the four test cases presented in this paper. The large bubble in the shape regimes of ellipsoidal and spherical cap can be accelerated due to the presence of small bubbles. The trapping of small bubbles in the large bubble wake zone has a minor

contribution to the increase of large bubble rise speed, while the sharper bubble nose and the lateral oscillation due to the presence of small bubbles can result in a great increase of the rise speed.

3.7. Effect of the initial positions for small bubble injections on the large bubble rise speed

Besides the flow rate of small bubble injections, the initial positions of small bubble injections also play significant effects on the rising behavior of the large bubble. To illustrate the effects of initial positions of small bubble injections, the total flow rate of small bubble injections is kept constant at $\dot{M}_{Pl} = 0.00619$, while the number of bubble injections is varied from 5 to 14 in the simulation tests. Every injection is assumed to have the same flow rate and distribute evenly across the channel width in each simulation test. The flow conditions for Test Case 3 ($Ar = 141.4$, $Eo = 40$) is selected for the numerical tests. Fig. 20 shows the predicted large bubble shapes and distributions of small bubble trajectories with different numbers of bubble injections varying at 5, 7, 10 and 14. When the number of small injections is fewer, the flow rate of each injection is stronger in term of flow rate. It creates stronger effects on the large bubble. The large bubble has larger deformation with sharper nose, higher degree of oscillation, and higher rise speed. Table 1 shows the variation of the large bubble rise speed and the small bubble concentration with the number of small bubble injections. When the number of bubble injections is high enough, the small bubbles are more uniformly distributed inside the channel and impose less effect on the rising behavior of the large bubble. As shown in Fig. 20 and Table 1, when the number of small bubble injections is 14, the rise speed of the large bubble is $Fr_B = 0.36$, which is slightly higher than that for the case (as shown in Fig. 11) without small bubble injection. The large bubbles in these two simulation cases also have similar shape.

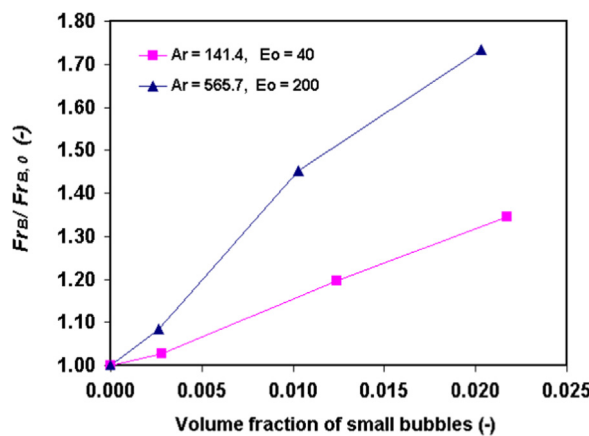


Fig. 19. Variation of the rise speed of large bubble with the volume fraction of small bubbles at relatively high Archimedes and Eötvös numbers.

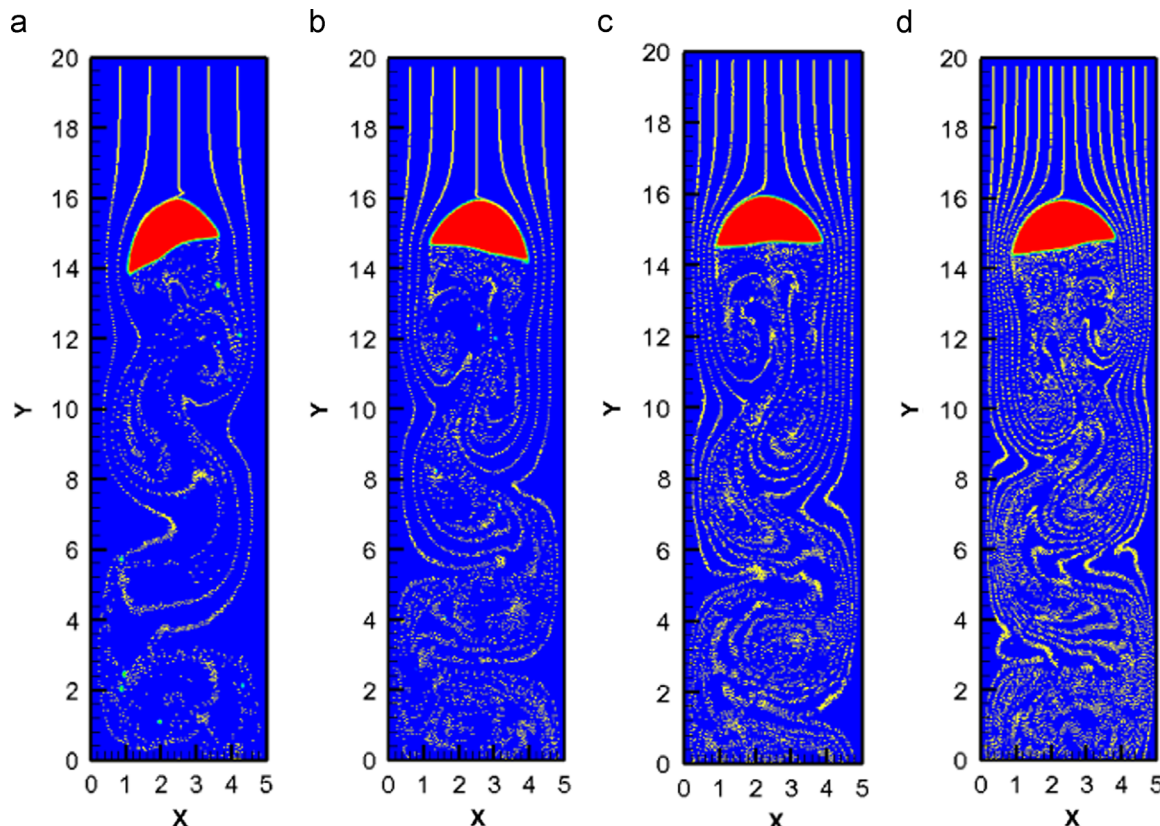


Fig. 20. Snapshots of predicted large bubble shape and trajectories of small bubbles with constant total injection rate ($\dot{M}_{Pl} = 0.00619$) and different numbers of initial bubble injections: (a) 5; (b) 7; (c) 10; (d) 14. $Ar = 141.4$, $Eo = 40$.

Table 1

Comparison on the effects of initial bubble injection numbers on the large bubble rising speed and small bubble concentration. $\dot{M}_{PI} = 0.00619$, $Ar = 141.4$, $Eo = 40$.

Number of bubble injections	0	5	7	10	14
Fr_B	0.358	0.434	0.417	0.369	0.36
α_b	–	1.12%	1.21%	1.28%	1.29%

4. Conclusions

A computational fluid dynamics based numerical model framework was proposed to simulate two-phase flows with multiple length-scale-interface structures, e.g. one large bubble and many small bubbles. In this numerical method, the large bubble is tracked using a volume of fluid (VOF) method, and the small bubbles are tracked using a discrete particle method (DPM). The Navier-Stokes equations for two-phase flow are solved for the viscous liquid and the large bubble phases as one continuous fluid. The trajectories and velocities of the small bubbles are solved in a Lagrangian manner. The two-way momentum coupling between the discrete bubbles and the continuous fluid phase is also taken into account in the simulation. To focus on the interaction between the large bubble and the small bubbles, a moving reference frame attached to the nose of the large bubble has been implemented.

To evaluate the model performance, this model was applied to simulating the interaction between a large bubble and many suspended small bubbles in a vertical channel under different bubble shape regimes. It is found that the small dispersed bubbles may impose important effects on the rise behavior of the large bubble. Both hindrance and acceleration effects have been revealed by the simulations. The hindrance effect occurs in the near-spherical bubble shape regime (relatively low Archimedes number and Eötvös number) where bubble coalescence is limited and no wake zone is formed behind the bubble. In this case, the rise speed of the large bubble decreases as the volume fraction of small dispersed bubbles increases. The acceleration effect occurs in the other bubble shape regimes e.g. oblate ellipsoidal and spherical cap (relatively high Archimedes number and Eötvös number) where significant deformation of the large bubble nose can occur due to the presence of small dispersed bubbles and a fairly large bubble wake zone is formed behind the large bubble. Due to the acceleration effect, the large bubble rise velocity increases when the volume fraction of small dispersed bubbles increases. In addition, the rising behavior of the large bubble is also affected by the initial injection pattern of small bubbles: the injection flow rate and the initial injection position. In principle, the findings revealed by the current modeling agree qualitatively with the observations in experiments and other simulations. It provides a foundation for the further development of a more comprehensive model. The physical mechanisms for the hindrance and acceleration of large bubble due to the presence of small bubbles are not discussed in detail in this paper, but this will be an interesting research topic for the future study using the proposed model.

The complex physics during the bubble–bubble interaction is not well understood so far. The interaction dynamics can be affected by bubble size scale, bubble velocity, fluid properties, surface tension, surface chemistry and surfactant. In this study, we focused on the interaction of different scaled bubbles, and some physical simplifications are made in the model so that the numerical model can be implemented at the current stage. For example, the collision of small bubbles (Darmana et al., 2006; Tomar et al., 2010) is not included, which may limit the model performance for the situation with high concentration of small bubbles. The physics of small bubble moving in the near region of

the larger bubble interface is simplified. A constant collision restitution coefficient (Fujasova-Zednikova et al., 2010) is assumed, and the effect of large bubble interface on the drag coefficient of small bubble (Liu and Schwarz, 2009; Verrelli et al., 2011) is not considered. Based on the simulation results of the current model, it can be believed that these simplifications can be modified and improved further in the current frame work in the future.

Acknowledgements

The author gratefully acknowledges the support from the project SPACE, supported by the Norwegian Research Council and the HORIZON II partners: Chevron, ConocoPhillips, ENI, ExxonMobil, Shell, Statoil, TOTAL and SPT Group. The author would also like to thank C. Lawrence, R. Skartlien and J. Nossen for the discussions and suggestions. The constructive comments and suggestions from the reviewers are also highly appreciated.

References

- Bhaga, D., Weber, M.E., 1981. Bubbles in viscous liquid: shapes, wakes and velocities. *J. Fluid Mech.* 105, 61–85.
- Clift, R., Grace, J.R., Weber, M.E., 1978. *Bubbles, Drops, and Particles*. Academic Press.
- Darmana, D., Deen, N.G., Kuipers, J.A.M., 2006. Parallelization of an Euler–Lagrange model using mixed domain decomposition and a mirror domain technique: application to dispersed gas–liquid two phase flow. *J. Comput. Phys.* 220, 216–248.
- Davies, R.M., Taylor, F.I., 1950. The mechanism of large bubbles rising through extended liquids and through liquids in tubes. *Proc. R. Soc. London, Ser. A* 200, 375–390.
- Ding, J., Gidaspow, D., 1990. A bubbling fluidization model using kinetic theory of granular flow. *AIChE J.* 36, 523–538.
- Fujasova-Zednikova, M., Vobecka, L., Vejrazka, J., Ruzicka, M.C., Drahos, J., 2010. Effect of liquid properties and solid material on bubble-wall attachment. In: Seventh International Conference on Multiphase Flow, ICMF 2010, Tampa, FL, USA.
- Garnier, C., Lance, M., Marie, J.L., 2002. Measurement of local flow characteristics in buoyancy-driven bubbly flow at high void fraction. *Exp. Therm. Fluid Sci.* 26, 811–815.
- Grace, J.R., 1973. Shapes and velocities of bubbles rising in infinite liquids. *Trans. Inst. Chem. Eng.* 51, 116–120.
- Hänsch, S., Lucas, D., Krepper, E., Höhne, T., 2012. A multi-field two-fluid concept for transitions between different scales of interfacial structures. *Int. J. Multiphase Flow* 47, 171–182.
- Hua, J., Langsholt, M., Lawrence, C., 2012. Numerical simulation of single elongated bubble propagation in inclined pipes. *Prog. Comput. Fluid Dyn.* 12, 131–139.
- Hua, J., Lou, J., 2007. Numerical simulation of bubble rising in viscous liquid. *J. Comput. Phys.* 222, 769–795.
- Hua, J., Stene, J.F., Lin, P., 2008. Numerical simulation of 3D bubbles rising in viscous liquids using a front tracking method. *J. Comput. Phys.* 227, 3358–3382.
- Krishna, R., Urseanu, M.I., van Baten, J.M., Ellenberger, J., 1999. Rise velocity of a swarm of large gas bubbles in liquids. *Chem. Eng. Sci.* 54, 171–183.
- Li, Y., Zhang, J., Fan, L.-S., 1999. Numerical simulation of gas–liquid–solid fluidization systems using a combined CFD–VOF–DPM method: bubble wake behavior. *Chem. Eng. Sci.* 54, 5101–5107.
- Liu, T.Y., Schwarz, M.P., 2009. CFD-based multiscale modelling of bubble–particle collision efficiency in a turbulent flotation cell. *Chem. Eng. Sci.* 64, 5287–5301.
- Oey, R.S., Mudde, R.F., van den Akker, H.E.A., 2003. Sensitivity study on interfacial closure laws in two-fluid bubbly flow simulations. *AIChE J.* 49, 1621–1636.
- Roghair, I., Lau, Y.M., Deen, N.G., Slagter, H.M., Baltussen, M.W., van Sint Annaland, M., Kuipers, J.A.M., 2011. On the drag force of bubble swarms at intermediate and high Reynolds numbers. *Chem. Eng. Sci.* 66, 3204–3211.
- Simonnet, M., Gentric, C., Olmos, E., Midoux, N., 2007. Experimental determination of the drag coefficient in a swarm of bubbles. *Chem. Eng. Sci.* 62, 858–866.
- Smolianski, A., Haario, H., Luukka, P., 2008. Numerical study of dynamics of single bubbles and bubble swarms. *Appl. Math. Model.* 29, 615–632.
- Stewart, C.W., 1995. Bubble interaction in low-viscosity liquids. *Int. J. Multiphase Flow* 21, 1037–1046.
- Sunol, F., González-Cinca, R., 2010. Rise, bouncing and coalescence of bubbles impacting at a free surface. *Colloids Surf., A* 365, 36–42.
- Tomar, G., Fuster, D., Zaleski, S., Popinet, S., 2010. Multiscale simulations of primary atomization. *Comput. Fluids* 39, 1864–1874.
- Tomiya, A., Celata, G.P., Hosokawa, S., Yoshida, S., 2002a. Terminal velocity of single bubbles in surface tension force dominant regime. *Int. J. Multiphase Flow* 28, 1497–1519.
- Tomiya, A., Tamai, H., Zun, I., Hosokawa, S., 2002b. Transverse migration of single bubbles in simple shear flow. *Chem. Eng. Sci.* 57, 1849–1859.

- Tsao, H.-K., Koch, D.L., 1997. Observations of high Reynolds number bubbles interacting with a rigid wall. *Phys. Fluids* 9, 44–56.
- van Sint Annaland, M., Deen, N.G., Kuipers, J.A.M., 2005. Numerical simulation of gas–liquid–solid flows using a combined front tracking and discrete particle method. *Chem. Eng. Sci.* 60, 6188–6198.
- Verrelli, D.I., Koh, P.T.L., Nguyen, A.V., 2011. Particle–bubble interaction and attachment in flotation. *Chem. Eng. Sci.* 66, 5910–5921.
- Yan, K., Che, D., 2010. A coupled model for simulation of the gas–liquid two-phase flow with complex flow patterns. *Int. J. Multiphase Flow* 36, 333–348.
- Yan, K., Che, D., 2011. Hydrodynamics and mass transfer characteristics of slug flow in a vertical pipe with and without dispersed small bubbles. *Int. J. Multiphase Flow* 37, 299–325.
- Yu, Z., Yang, H., Fan, L.-S., 2011. Numerical simulation of bubble interactions using an adaptive lattice Boltzmann method. *Chem. Eng. Sci.* 66, 3441–3451.